

Supplementary Materials for “Powering a Microprocessor by Photosynthesis”

This PDF file includes:

Figs. S1 to S17

Table S1

Materials and Methods

Supplementary References

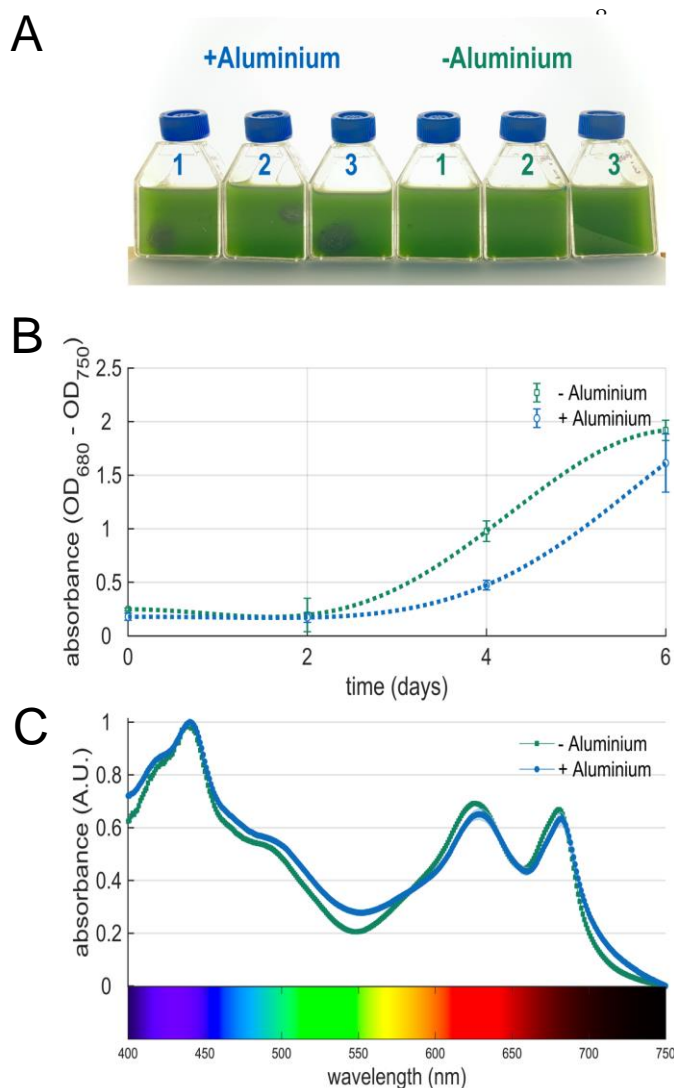


Fig. S1. Growth of *Synechocystis* in the presence of aluminium wool. **A)** Flasks of *Synechocystis* with or without aluminium (three replicates, six days after inoculation). **B)** Growth curves for *Synechocystis* with or without aluminium. **C)** Normalised absorption spectra for cell suspension of *Synechocystis* with or without aluminium.



Fig. S2. Aluminium wool used in this study. **A,B)** Photographs of the filaments of aluminium at two different magnifications. The filaments are up to 300 mm long and have a diameter varying from 100 μm to 300 μm .

40
41
42
43
44
45
46
47

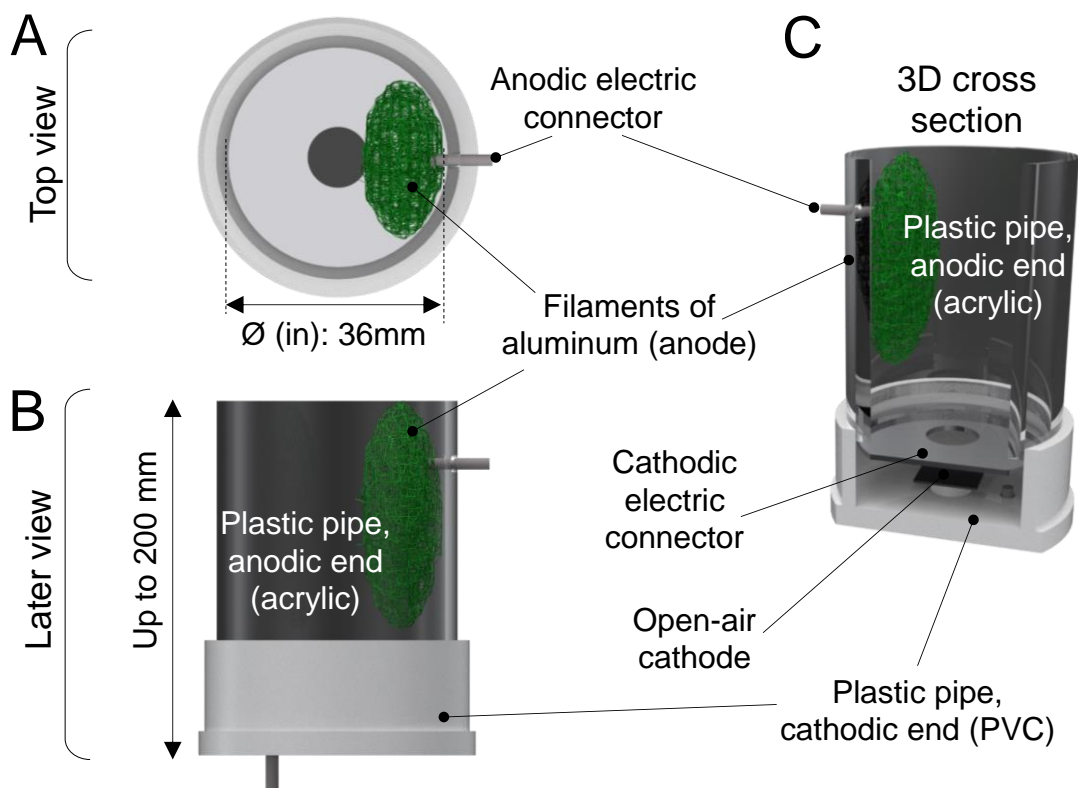
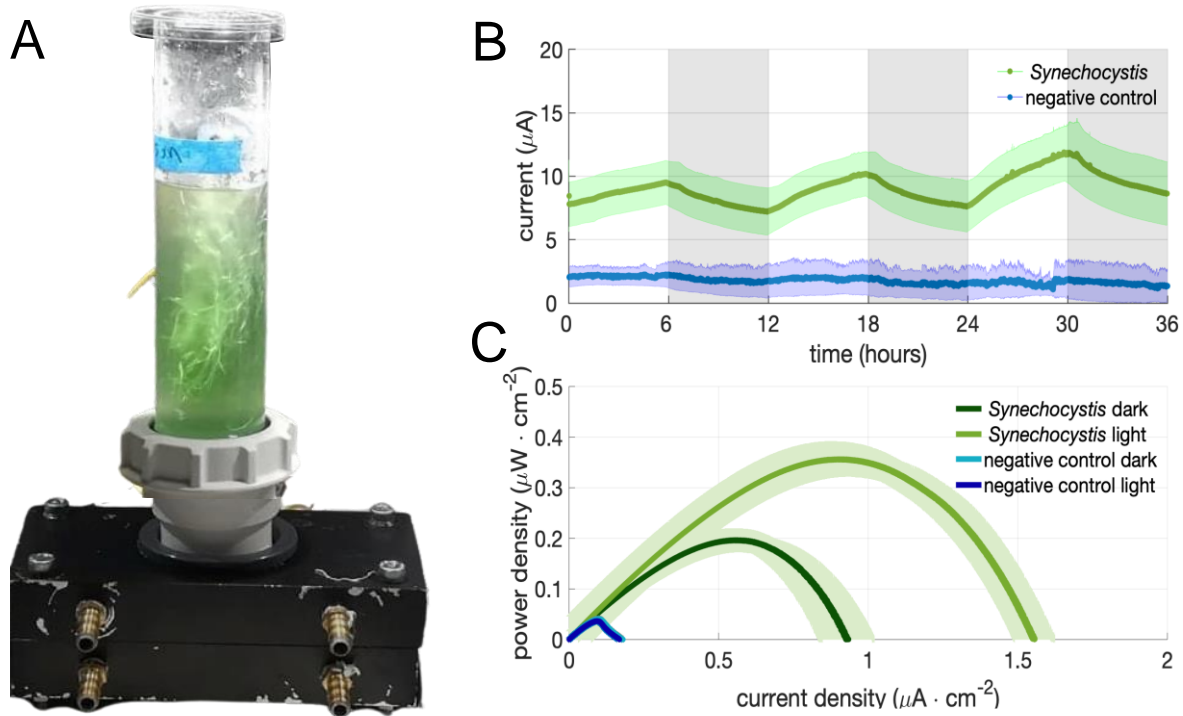


Fig. S3. Structure of the prototype Al-BPV system. **A,B)** Diagram of the key components and dimensions forming the prototype Al-BPV system, top and lateral view respectively. **C)** 3D cross section of the of prototype Al-BPV system displaying the key components.

48
49
50
51



53

54

55

56

57

58

59

60

61

62

63

64

65

66

67

68

69

70

71

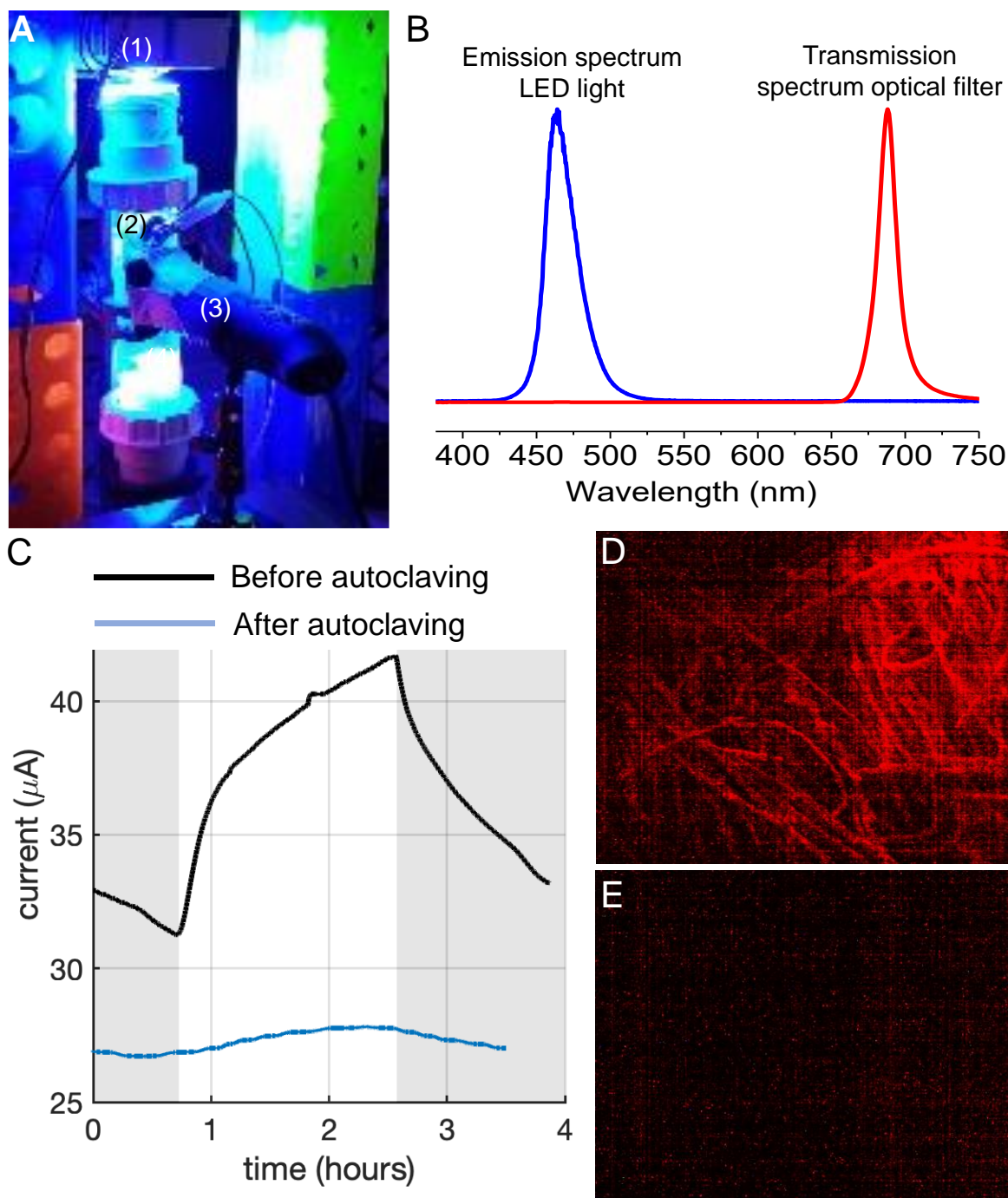
72

73

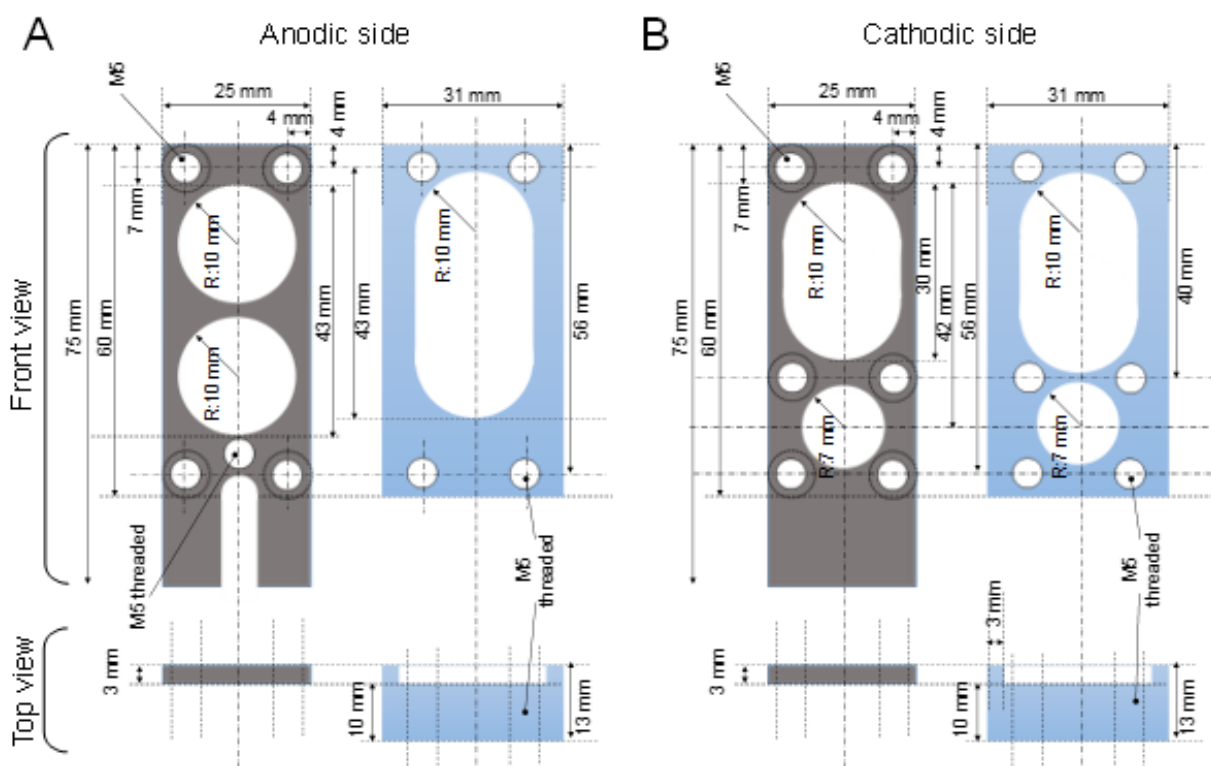
74

75

Fig. S4. Performance of the prototype Al-BPV system. **A)** Photo of the prototype Al-BPV system used for laboratory testing and operated with *Synechocystis*. **B)** Current generated by aluminium anodes colonised by *Synechocystis* (green trace) or for abiotic negative control (blue trace) in the prototype Al-BPV. White and dark panels represent periods of light and dark respectively. Current was measured using a MultiEmStat Potentiostat in chronoamperometry mode with bias potential of 0V. **C)** Power curves for prototype Al-BPV systems under dark (dark green trace) and light (light green trace) respectively (n=3). The green shadow represents the standard deviation of the mean (n=3). Blue traces indicate the abiotic negative controls under dark (light blue trace) and light (dark blue trace) respectively (n=3). Current and power intensity were normalised by the total illuminated surface of the BPV (10.2 cm²) to calculate the reported current and power densities. Illumination was provided by warm-white LED placed at the top. The measured peak power densities per unit area for *Synechocystis* in dark and light, respectively, were $0.197 \pm 0.023 \mu\text{W cm}^{-2}$ and $0.361 \pm 0.034 \mu\text{W cm}^{-2}$. The measured peak power densities per unit area for the negative control in dark and light, respectively, were $0.041 \pm 0.001 \mu\text{W cm}^{-2}$ and $0.037 \pm 0.003 \mu\text{W cm}^{-2}$. Using the above peak power densities, a two-sample student t-test (ttest2 in Matlab R2021) was performed to assess the statistical significance of the differences in peak power densities between anodes with *Synechocystis* and autoclaved anodes (negative control). The test comparing *Synechocystis* and negative control anodes in the light rejected the null hypothesis that there was no difference ($H = 0$) and returned a p-value (significant at the 5% level) of 0.0051. The test comparing *Synechocystis* and negative control anodes in the dark rejected the null hypothesis ($H = 0$) and returned a p-value (significant at the 5% level) of 0.0169.

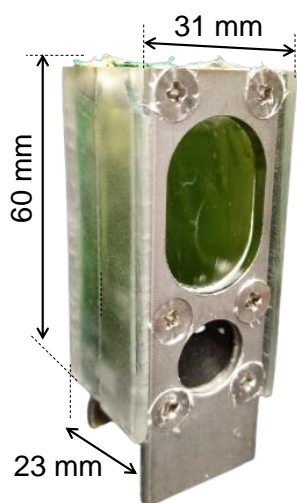


76 **Fig. S5.** Autofluorescence and current output measured from a prototype Al-BPV system 12
 77 months old **A)** Experimental set-up used to observe autofluorescence. LED light source (1); Al-
 78 BPV system (2); optical filter (3); digital camera (4). **B)** Emission spectrum of the LED light
 79 ($\lambda=475\text{nm}$, blue line) and transmission spectrum ($\lambda=688\text{nm}$, red line) of the optical filter used.
 80 **C)** Current output generated by an Al-BPV system before (black) and after autoclaving (blue).
 81 The grey and white backgrounds represent periods of dark and light respectively. **D)**
 82 Autofluorescence emitted by an aluminium anode taken with an optical filter in front of the
 83 digital microscope. **E)** Autofluorescence emitted by an autoclaved aluminium anode taken with
 84 an optical filter in front of the digital microscope.



85
86
87
88
89

Fig. S6. Diagram of the main components of the compact Al-BPV system used to power the CPU. **A,B)** anodic and cathodic side respectively. The grey and the light blue shades denote stainless-steel and acrylic respectively. The screws holding the components together are not shown in this diagram.



Compact Al-BPV

Width*: 31 x 23 mm
Height*: 60 mm

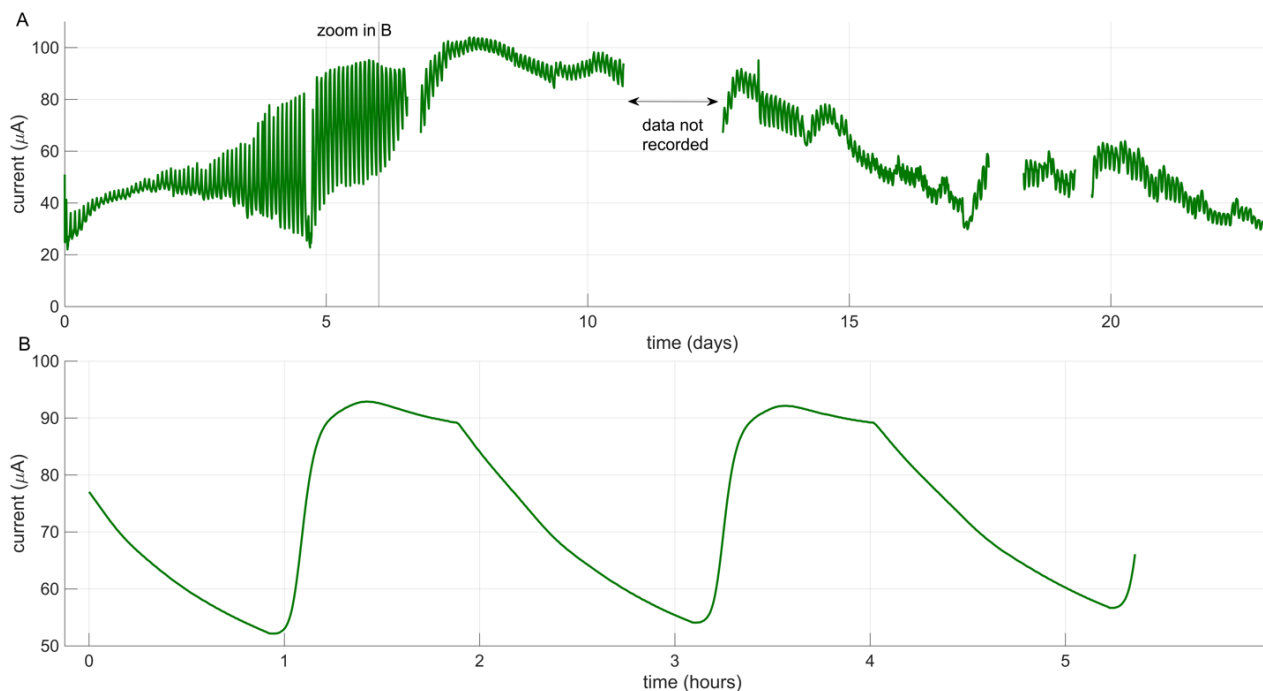
Anode: Aluminum filament (0.7 g)
Cathode: Carbon paper-Pt (active area \varnothing 7 mm)
Body: acrylic block and PTFE film
Electric connectors: stainless-steel metal plates

*dimension of the external system

90
91
92
93
94
95
96
97
98
99
100
101
102

103
104
105
106

Fig. S7. Compact Al-BPV system used to power the ultra-low-power processor: dimensions and materials. The body of the Al-BPV was made using acrylic, polytetrafluoroethylene (PTFE) and stainless-steel (S/S) plates. The aluminium anode is fastened to the metal plate using 4 mm stainless-steel screws and washers.



107

108 **Fig. S8.** The compact Al-BPV (**Fig.1C,D** and **Fig.S6,7**) was first tested in a controlled laboratory
 109 environment (20-22 °C and white-warm LED light at $\sim 500 \mu\text{E m}^{-2} \text{s}^{-1}$). The peak power ($4.2 \mu\text{W}$
 110 cm^{-2}) and max current ($17.2 \mu\text{A cm}^{-2}$) per unit area of the compact Al-BPV determined under
 111 laboratory conditions (**Fig.1E**) were comparable to values obtained with other BPV systems.
 112 Chronoamperometry of the compact Al-BPV system in a laboratory-controlled environment. (Data
 113 recording was lost from day 11 to day 13.) **A**) Current intensity as a function of time during ca. 23
 114 days. **B**) A zoomed-in inset of data in A plotted with hourly resolutions. The LED that illuminated
 115 the BPV was programmed to emit light-dark cycles with a period of 2 hours.

116

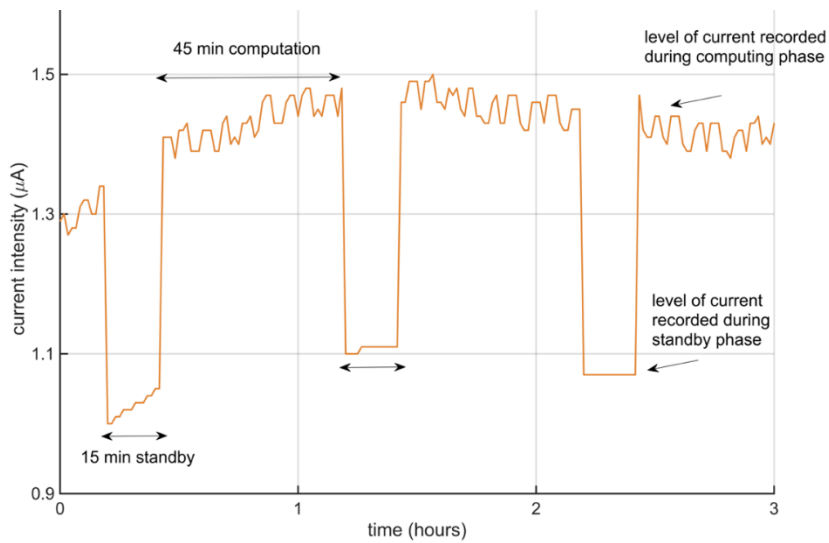
117

118

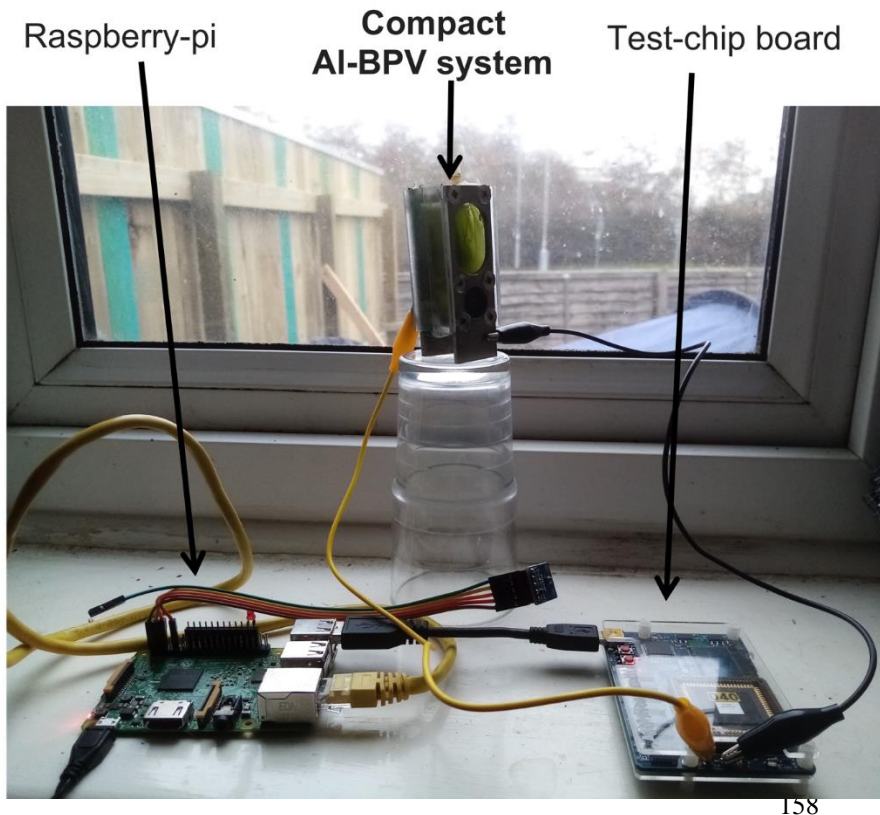
119

120

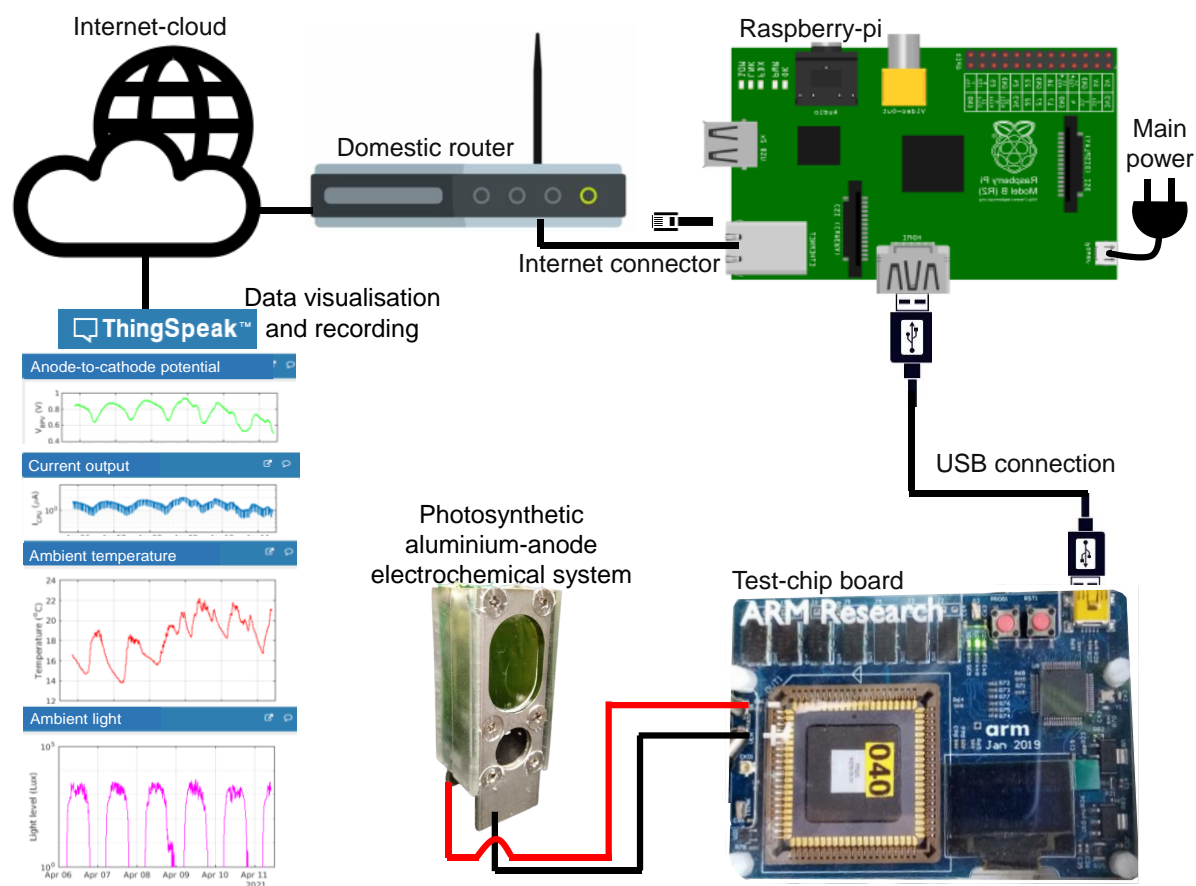
121



135 **Fig. S9.** Example of current recording during the operation of the Cortex-M0+ processor. Variation
 136 of the current drawn from the compact AI-BPV system during the CPU cycle of alternating
 137 operation (45 minutes in computing mode followed by 15 minutes in standby).
 138



159 **Fig. S10.** Domestic environment where the experimental tests were conducted. The compact AI-
 160 BPV was placed at the window sill in a living room of a domestic property. The location is in
 161 Cambridge (UK), latitude: 52.23 / 52°14'0"N; longitude: 0.1329 / 0°7'58"E.



162
163
164
165
166
167
168
169
170
171
172
173
174
175
176
177
178
179
180

Fig. S11. Compact AI-BPV system powering the processor: Data recording and visualisation. The photosynthetic aluminium-anode electrochemical system powered the Cortex-M0+ processor. The photosynthetic aluminium-anode electrochemical system powers only the Cortex-M0+ processor in the test chip, which consumes a minimum of $0.3 \mu\text{W}$ (@0.3V). The test-chip board verifies the operation of the processor and measures the potential and intensity of the electrical output of the photosynthetic aluminium-anode electrochemical system. Data are transferred to the Internet-cloud via a Raspberry-pi/router. The rest of the test-chip other than the Cortex-M0+ processor, all other electronic components in the test-chip board, Raspberry-pi and router are powered by the mains power. The ThingSpeak™ platform is used to record and visualise the data (<https://thingspeak.com/channels/1033008>).

181
 182
 183
 184
 185
 186
 187
 188
 189
 190
 191
 192
 193
 194
 195
 196
 197
 198
 199
 200
 201
 202
 203
 204
 205
 206
 207
 208
 209
 210
 211
 212
 213
 214
 215
 216
 217
 218
 219
 220

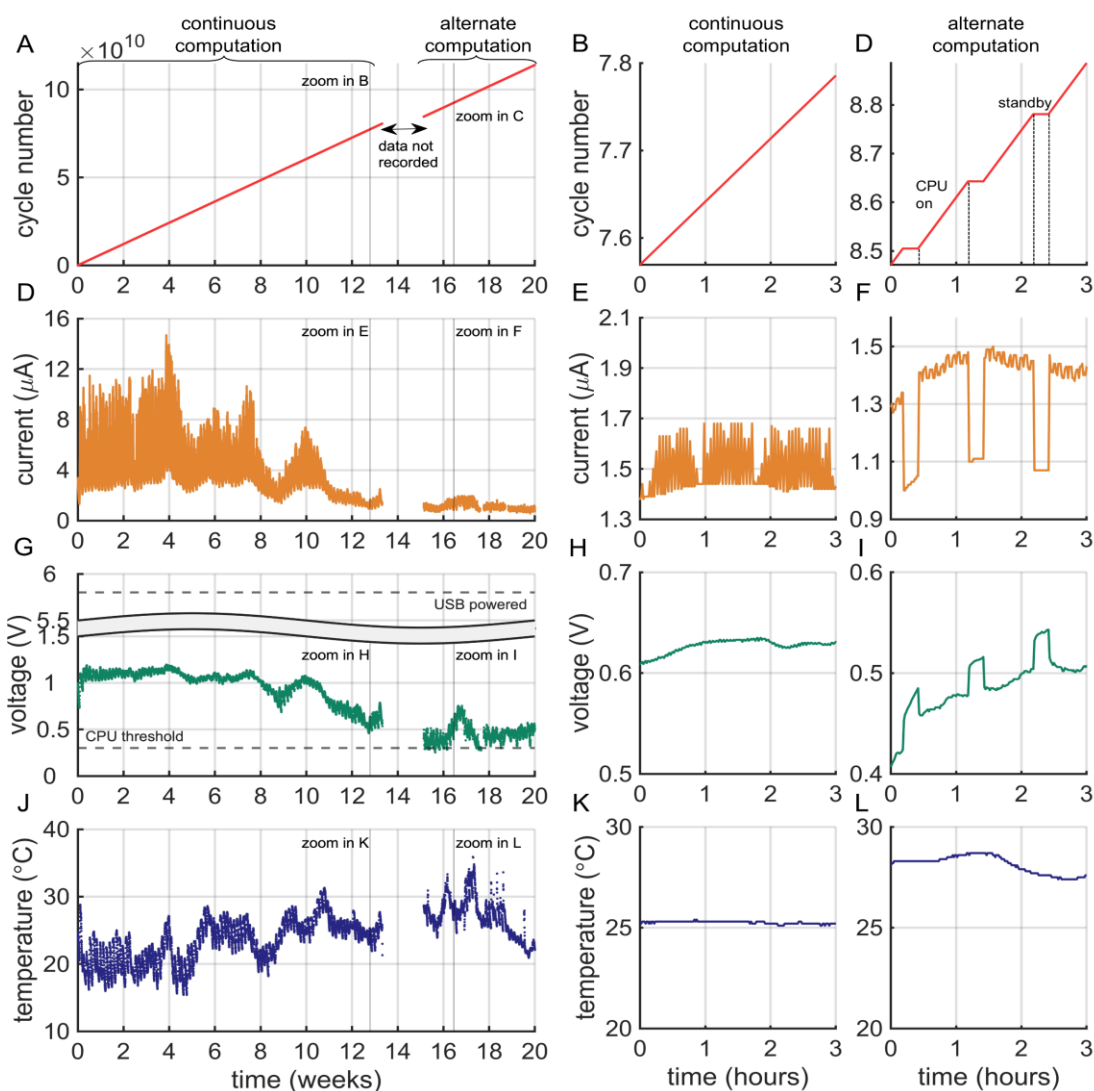
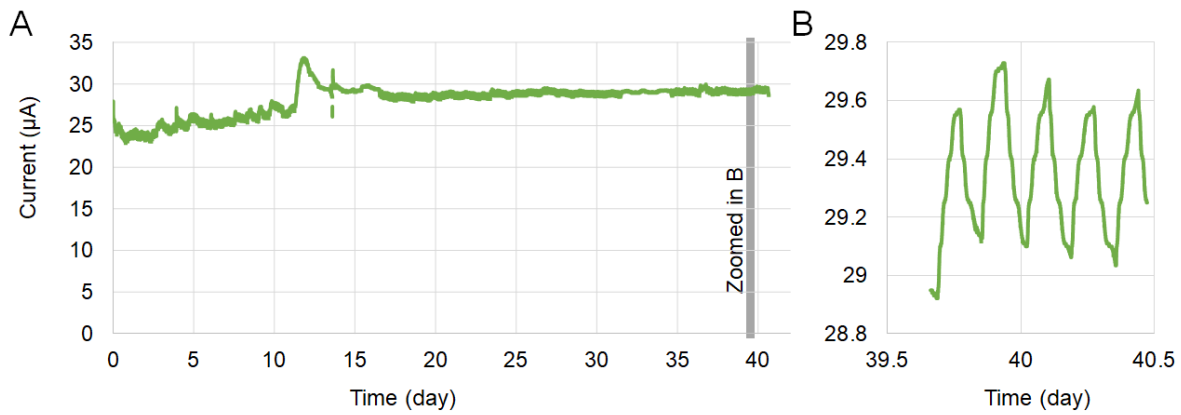


Fig. S12. Powering the Arm Cortex-M0+ processor by the compact AI-BPV system in a domestic environment. The experiment included a first phase (week 0 to week 13) of continuous computation followed by a second phase (week 15 to week 20) during which the CPU alternated in cycles from 45 minutes of computation to 15 minutes of standby. The data presented in the left column (**A,D,G** and **J**) show the entire experimental run. The data presented in the centre column (**B,E,H** and **K**) show three hours of recording taken from an arbitrary point (in continuous computation mode) of the left column. The data presented in the right column (**C,F,I** and **L**) show three hours of recording taken from an arbitrary point of the centre column (in alternate computation mode). **A-C)** Cumulative number of cycles of computation events performed by the CPU. **D-F)** Current generated by the BPV device. **G-I)** Potential difference between the anode and cathode of the BPV device. The dotted line indicates the threshold of potential below which the CPU will stop working. The section above the line break in the y axis indicates the voltage range (5.5-6 V) that would be recorded if the BPV failed to power the CPU (the CPU would then be USB powered). **J-L)** environmental temperature measured by a probe integrated into the test-chip.



222 **Fig. S13.** Current output generated under constant cycles of light and dark by an Al-BPV system
223 that had been operating for more than two years. The light and dark cycle was arbitrarily fixed at
224 2h:2h **A)** Circa 40 days of continuous recording. **B)** Several hours of recording taken from an
225 arbitrary point (depicted by the grey-shaded regions) in panel **A**.

226

227

228

229

230

231

232

233

234

235

236

237

238

239

240

241

242

243

244

245

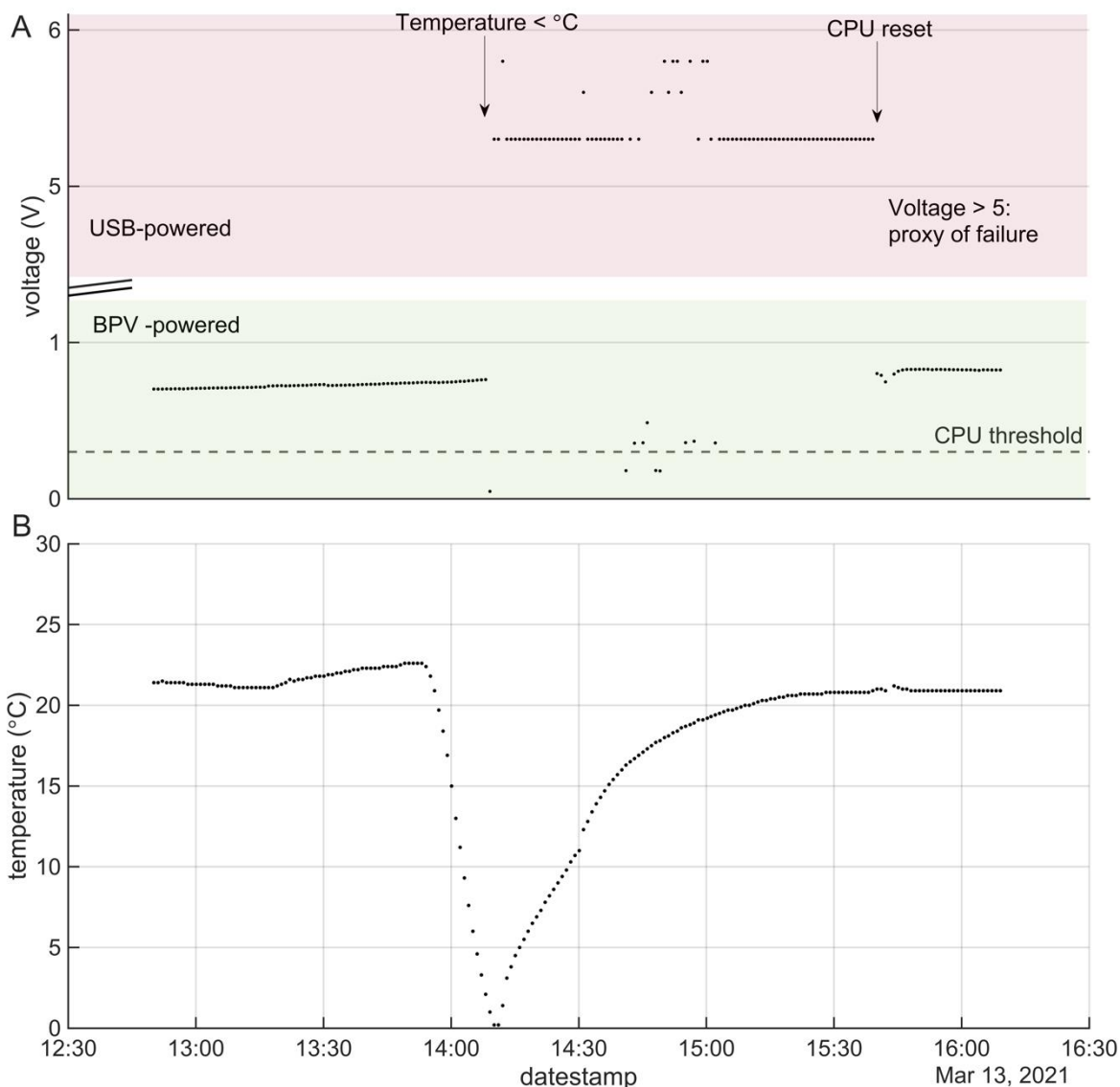
246

247

248

249

250



251 **Fig. S14.** Change in voltage (A) and temperature (B) when the compact AI-BPV fails to power the
 252 processor. Those data are zoomed from **figure 2G** and **2M** respectively. The pink panel indicates
 253 where the processor is powered from an external supply, and the green indicates where it is
 254 powered by the AI-BPV. The failure was deliberately induced by lowering the ambient
 255 temperature (B) below 5 $^{\circ}\text{C}$ with an ice-pack. In this instance, the software controlling the
 256 operation of the CPU triggered to switch the power of the processor from the AI-BPV to another
 257 electricity supply via a USB which is indicated by recording a voltage >5V.

258
 259
 260
 261
 262
 263



264
265 **Fig. S15.** Filaments from an aluminium anode taken from a mature Al-BPV system several months
266 old. **A-E)** Photograph of the filaments of aluminium anode and matrix (aluminium hydroxide and
267 extracellular components) taken with a stereo microscope at various magnifications and
268 orientations. The filaments have diameter ranging from 0.2 to 0.4 mm.
269
270
271
272
273
274
275
276
277
278
279
280
281

282
283
284
285
286
287
288
289
290
291
292
293
294
295
296
297
298
299
300
301
302
303
304
305
306
307
308
309
310
311
312
313
314
315
316
317
318
319
320

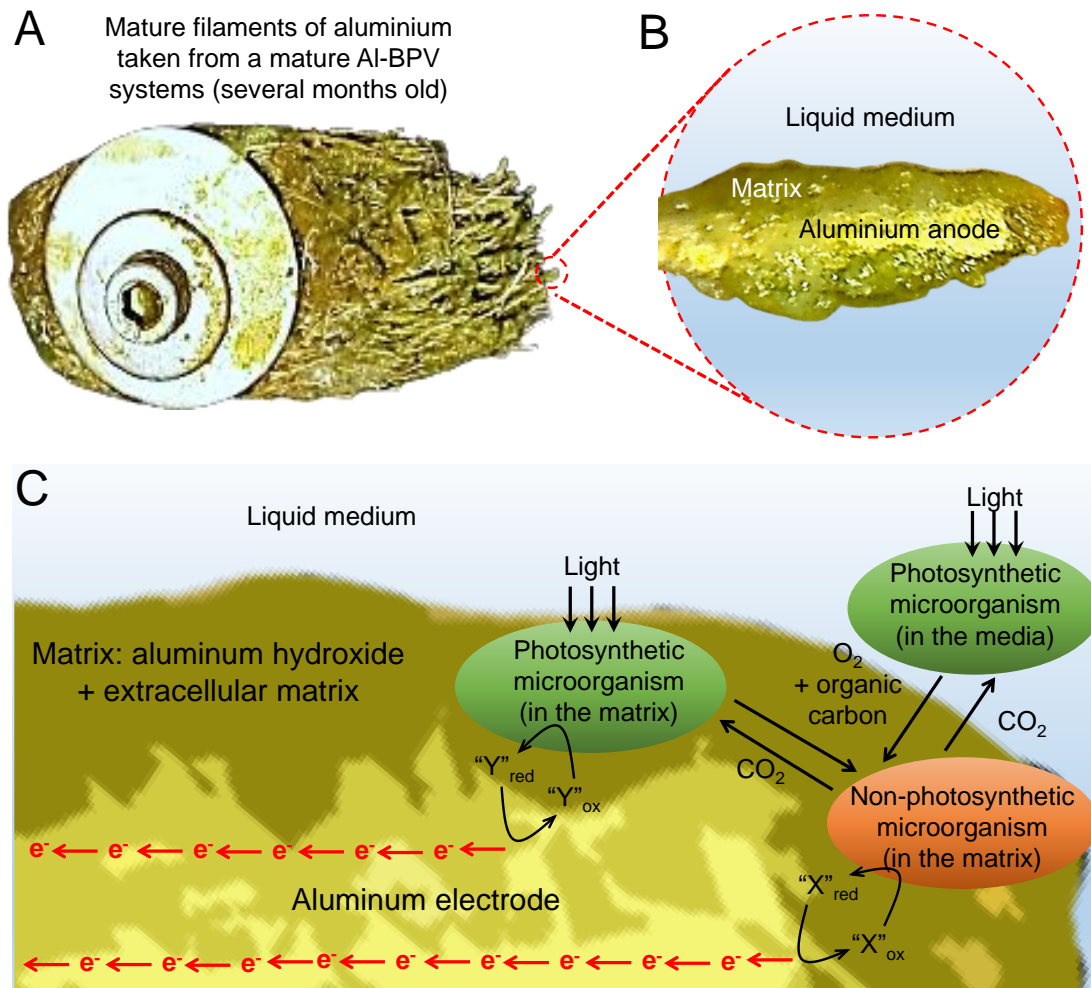
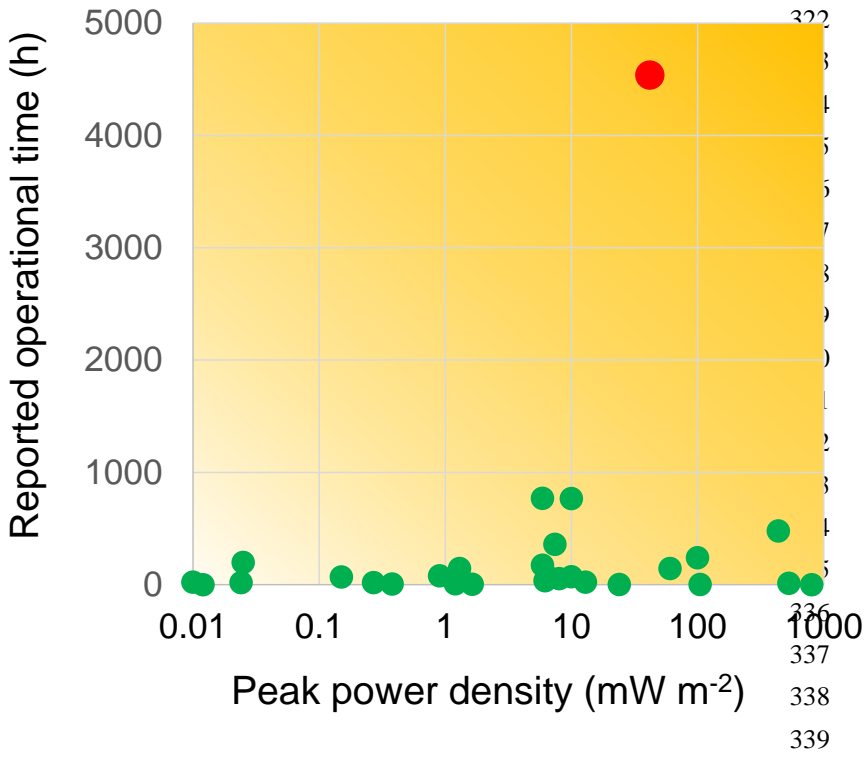


Fig.S16. Mechanism of electron transport. **A)** The aluminium anode taken from a mature Al-BPV system. **B)** Magnification of a filament of the aluminium anode taken from a mature Al-BPV system with the position of the actual anode and the matrix (aluminium hydroxide and extracellular components) annotated. **C)** Proposed mechanisms of electron transport within the mix of aluminium hydroxide and extracellular matrix.

321



340

341

342 **Fig. S17.** The performance of our AI-BPV system (red marker) in terms of operational time *versus*
343 peak power density, compared with the published state of the art of this technology. The data are
344 given in **ST1**.

345

346

347

348

349

350

351

352

353

354

355

356

357

358

359

360

361
362
363

Table S1. List of publications consulted to generate **figure S17**. The operational time reported for the compact-AI-BPV in this present study was calculated based on the data presented in **figure 2**. Data not available are marked with n.a.

| References | Ref | Peak power output (mW m ⁻²) | Max operational time (h) |
|---|-----|---|--------------------------|
| | | | |
| Fu Chun-Chong, <i>et al.</i> , <i>Bioresource Technology</i> , 2009, 100 , 4183–4186 | 1 | 1.64 | 5 |
| Zou Yongjin, <i>et al.</i> , <i>Biotechnology & Bioengineering</i> , 2009, 104 , 5 | 2 | 1.3 | 144 |
| Fu Chun-Chong, <i>et al.</i> , <i>Biochemical Engineering Journal</i> , 2010, 52 , 175–180 | 3 | 6.5 | 70 |
| Pisciotta John M., <i>et al.</i> , <i>PLoS ONE</i> , 2010, 5 , 5, e10821 | 4 | 5.9 | 770 |
| Zou Yongjin, <i>et al.</i> , <i>Bioelectrochemistry</i> , 2010, 79 , 50–56 | 5 | 5.9 | 175 |
| Bombelli P., <i>et al.</i> , <i>Energy & Environmental Science</i> , 2011, 4 , 11, 4690-4698 | 6 | 1.2 | 8 |
| McCormick A. J., <i>et al.</i> , <i>Energy & Environmental Science</i> , 2011, 4 , 11, 4699-4709 | 7 | 10 | 768 |
| Thorne R., <i>et al.</i> , <i>J. Mater. Chem.</i> , 2011, 21 , 18055 | 8 | 24 | 2 |
| Bombelli P., <i>et al.</i> , <i>PCCP</i> , 2012, 14 , 12221–12229 | 9 | 0.024 | 20 |
| Madiraju K. S., <i>et al.</i> , <i>Bioresource Technology</i> , 2012, 110 , 214–218 | 10 | 0.27 | 20 |
| Raman K. <i>et al.</i> , <i>Applied Energy</i> , 2012, 100 , 100–105 | 11 | 0.82 | n.a. |
| Bradley R.W., <i>et al.</i> , <i>PCCP</i> , 2013, 15 , 32, 13611-13618 | 12 | 0.181 | n.a. |
| Chen W. J., <i>et al.</i> , <i>ACS Appl. Mater. Interfaces</i> , 2013, 5 , 11123–11128 | 13 | 0.15 | 70 |
| Inglesby A. E., <i>et al.</i> , <i>PCCP</i> , 2013, 15 , 6903-691 | 14 | 0.025 | 200 |
| Lan J.C.W., <i>et al.</i> , <i>Biochemical Engineering Journal</i> , 2013, 78 , 39– 43 | 15 | 12.95 | 24 |
| Lin C.C., <i>et al.</i> , <i>Bioresource Technology</i> , 2013, 135 , 640–643 | 16 | 10 | 72 |
| Luimstra V.M., <i>et al.</i> , <i>J Appl Phycol</i> , 2014, 26 , 15–23 | 17 | 6.2 | 36 |
| Schneider K., <i>et al.</i> , <i>Philosophical Transactions A</i> , 2016, 374 , 20150080 | 18 | 7.4 | 360 |
| Samsonoff N., <i>et al.</i> , <i>Appl. Phys. Lett.</i> , 2014, 104 , 043704 | 19 | 0.012 | 1 |
| Sekar N., <i>et al.</i> , <i>Phys. Chem. Chem. Phys.</i> , 2014, 16 , 7862-7871 | 20 | 100 | 240 |
| Ng F. L., <i>et al.</i> , <i>PLoS ONE</i> , 2014, 9 , 5, e97643 | 21 | 0.31 | n.a. |
| Ng F. L., <i>et al.</i> , <i>Scientific Report</i> , 2014, 4 , 7562 | 22 | 0.27 | n.a. |
| Bombelli P., <i>et al.</i> , <i>Advanced energy materials</i> , 2015, 5 , 2, 1401299 | 23 | 105 | 2 |
| Huang L.F., <i>et al.</i> , <i>Int. J. Mol. Sci.</i> , 2015, 16 , 19308-19325 | 24 | 0.01 | 24 |
| S. Yoon <i>et al.</i> , <i>NEMS</i> , 2014, 391-398 | 25 | 0.9 | 80 |
| Wei X., <i>et al.</i> , <i>IEEE SENSORS</i> , 2016, 1-3 | 26 | 60.5 | 144 |
| Sawa M., <i>et al.</i> , <i>Nature communications</i> , 2017, 8 , 1, 1-10 | 27 | 0.38 | 7 |
| Liu L. and Choi S., <i>Lab. Chip</i> , 2017, 17 , 3817–3825 | 28 | 438 | 480 |
| Saar K. L. <i>et al.</i> , <i>Nature energy</i> , 2018, 3 , 1, 75-81 | 29 | 530 | 12 |
| Kim, M.J., <i>et al.</i> , <i>Journal of Power Sources</i> , 2019, 412 , 301-310 | 30 | 806 | 1 |
| This present study | | 42 | 4536 |

364
365
366

367 **Materials and Methods**

368 ***Synechocystis* culture and growth**

369 Wild-type *Synechocystis* sp. PCC6803 (hereafter *Synechocystis*) was routinely cultured in BG-11
370 medium³¹ supplemented with 10 mM NaHCO₃ and maintained in sterile conditions at (30 ± 2) °C
371 under continuous moderate light of 40 μmol photons m⁻² s⁻¹ and shaking at 160 revolutions per
372 minute (rpm.). A bench-top centrifuge (5,000 rpm for 3 min) was used to concentrate the cells. The
373 concentration of chlorophyll in samples was determined spectrophotometrically from the optical
374 density values at 680 nm and 750 nm as described previously³² (Lea-Smith *et al.*, 2013).

376 **Growth Assays in the Presence of Aluminium**

377 To perform growth assays in the presence of aluminium (**Fig.S1**), cultures were prepared by
378 inoculating 3 independent colonies growing on an agar plate into 20 mL of BG11 medium³¹ in 50
379 mL NuncTM flasks. Cultures were grown photoautotrophically in an Infors incubator at 30 °C under
380 40 μE m⁻² s⁻¹ continuous white fluorescence light, shaking at 120 rpm. After 5 days, 5 mL from
381 each culture was diluted in 35 mL of BG11 in three new Nunc flasks, resulting in three replicates
382 (each containing an initial OD₇₅₀ ≅ 0.25) for growth without aluminium. To quantify growth in
383 the presence of aluminium, 1.5 grams of fine-grade aluminium wool (Rogue River Tools, USA)
384 (**Fig.S2**) were weighed and inserted at the bottom of three additional flasks. These flasks were then
385 filled with 5 mL of precultures and 35 mL of sterile BG11 medium. Before inserting the aluminium
386 wool in the sterile flasks, aluminium filaments were cleaned according to a protocol described by
387 Kumari *et al.* (2019)³³. Briefly, dirt was removed by etching electrodes in a 7.5 wt% solution of
388 NaOH, then the electrodes were cleaned in concentrated HNO₃, thoroughly rinsed in deionised
389 water and then autoclaved. The 6 flasks were then grown for six days under photoautotrophic
390 conditions in an Infors incubator at 30 °C under 40 μE m⁻² s⁻¹ continuous white light, shaking at
391 120 rpm. Every other day, optical density measurements were performed using a Shimadzu UV-
392 1800 (Shimadzu, United Kingdom) spectrophotometer, recording absorbance spectra between
393 400-750 nm, using BG11 and BG11 + aluminium wool as blanks.

395 **Colonising the aluminium anode with *Synechocystis***

396 Electrochemical characterisation of *Synechocystis* biofilms was performed on previously
397 colonised aluminium electrodes transferred into single-chamber, two-electrode biophotovoltaic

398 devices. To colonise the aluminium wool electrodes, a ~29L photobioreactor was constructed
399 using transparent fish tanks (40 x 25.5 x 28cm) as reactor vessels. Each tank contained 18
400 aluminium anodes stacked in parallel using a stainless steel bar and was filled with 20 L of sterile
401 BG11 medium. Each aluminium anode was assembled with 1.5 grams of 10 cm long fine-grade
402 aluminium wool (Rogue River Tools, USA) (**Fig.S2**). The aluminium threads were held together
403 by marine-grade stainless-steel washers and bolts. Each tank was bubbled with filtered air pumped
404 using air pumps and plastic tubing and was stirred with magnetic stirrer bars. Each tank was
405 illuminated from the top by two 9W LED bars (RS components, United Kingdom). Before
406 inoculating the reactor with cells, the tanks were sterilised with 70% ethanol and UV radiation.
407 The aluminium electrodes were cleaned according to the protocol described above (Kumari et al.
408 2019). After two weeks of operation at room temperature at 12 hours light /6 hours dark cycles,
409 individual electrodes from the reactor vessel were transferred into prototype Al-BPV
410 electrochemical cells.

411

412 **Developing the prototype Al-BPV**

413 The prototype Al-BPV were assembled as follows. The aluminium anodes were formed as
414 previously described and transferred into a single-chamber prototype. The chamber was made with
415 a Perspex tube of 40 mm external diameter, 36 mm internal diameter and 200 mm long. Each
416 aluminium anode was assembled with 1.5 grams of 10 cm long fine-grade aluminium wool (Rogue
417 River Tools, USA) (**Fig.S2**). The aluminium threads were held together and secured to the Perspex
418 tube by marine-grade stainless-steel washers and bolts (RS Components, UK). The cathode
419 consisted of coated carbon paper/Pt (loading 3 mg cm⁻², Alfa Aesar 45372 Hydrogen
420 Electrode/Reformate, USA). The cathode was secured at one end of the Perspex tube with a
421 [McAlpine T28M Straight Connector 40mm x 40mm](#) (ScrewFix, UK), a rubber O-ring and a 36mm
422 diameter stainless-steel washers (RS Components, UK) to ensure a secure connection (**Fig.S3** and
423 **Fig.S4A**). The prototype Al-BPV were filled with ~200 mL of sterile BG11 medium.

424

425 **Electrochemical characterisation of prototype Al-BPV in laboratory-controlled environment**

426 The electrical output of the prototype Al-BPVs containing individual aluminium electrodes was
427 measured and recorded with a multi-channel MultiEmStat3 Potentiostat (PalmSense, UK) in
428 chronoamperometry mode at applied bias potential of 0 V. Recordings were taken every 5 seconds

429 for ~36 hours (**Fig.S4B**). Experiments were conducted at 12 hours cycle (6 hour light / 6 hour
430 dark), illuminated from the top by a 3W warm-white LED (RS components, UK). The
431 experimental run was conducted in a laboratory-controlled environment at 22 ± 2 °C throughout
432 the characterization process. Experiments were repeated at least three times with three
433 independently colonised electrodes.

434 After chronoamperometric measurements, linear sweep voltammetry from -0.8V to 0V was
435 performed at scan rate of 0.0001 V/s both in dark and light conditions, illuminated from the top by
436 a 3W LED (RS components, United Kingdom) to derive the peak power and maximum current as
437 shown in the power curved (**Fig.S4C**). The experimental run was conducted in a laboratory-
438 controlled environment at 22 ± 2 °C throughout the characterization process.

439

440 **Effect of DCMU on the photo-current**

441 For photocurrent inhibition experiments (**Fig.1B**), 30 μ L of 3-(3,4-dichlorophenyl)-1,1-
442 dimethylurea (DCMU, CAS number: 330-54-1; Sigma, UK) from a 0.1 M stock (final
443 concentration = 15 μ M) was added into the anodic chamber of the BPV whilst current output was
444 measured and recorded with a multi-channel MultiEmStat3 Potentiostat (PalmSense, UK) in
445 chronoamperometry mode at applied bias potential of 0 V. Experiments were conducted with a 4
446 hours cycle (2 hour light / 2 hour dark), illuminated from the top by a 3W LED (RS components,
447 UK). The experimental run was conducted in a laboratory-controlled environment at 22 ± 2 °C
448 throughout the characterization process (**Fig.1B**)

449

450 **Autofluorescence and current output**

451 Autofluorescence was observed from a prototype Al-BPV system equipped with an aluminium
452 anode colonised with photosynthetic microorganisms several months old. The experiment was
453 conducted using a setup (**Fig.S5A**) including a custom-made light emission device fitted with a
454 LZC-00MC40 RGB LED light (RS Components, UK). Blue light ($350 \mu\text{E m}^{-2} \text{s}^{-1}$, peak emission
455 at $\lambda=475\text{nm}$) was shone from the top into the anodic chamber of the Al-BPV system through the
456 transparent Perspex. The LED light spectra (**Fig.S5B**, blue line) was measured using a
457 Spectrometer USB2000+UV-VIS detector (Ocean Optics, US). A digital camera was placed
458 behind an optical filter and focused on the aluminium filaments of the colonised anode. The
459 transmission spectrum of the optical filter peaked at $\lambda=688\text{nm}$ (**Fig.S5B**, red line).

460 Autofluorescence was observed whilst current output was measured in chronovoltammetry mode
461 with an external load of 10 k Ω (**Fig.S5C** black line) using a multi-channel MultiEmStat3
462 Potentiostat (PalmSense, UK) as previously described. To enhance the autofluorescence 10 frames
463 were digitally combined to form the image shown in **Figure S5D**.

464 The aluminium anode colonised with photosynthetic microorganisms was removed from the
465 anodic chamber of the Al-BPV system and autoclaved (20 min, 121 °C, 15 psi). The autoclaved
466 electrode was reinstalled in the anodic chamber of the Al-BPV system and used to re-assess the
467 current output (**Fig.S5C** blue line) and autofluorescence (**Fig. S5E**) measured as for the aluminium
468 electrode before autoclaving.

469

470 **Developing a compact Al-BPV**

471 The body of the compact Al-BPV was made by a block of acrylic (Engineering & Design Plastics
472 Ltd, UK) 60mm high and 31 x 23 mm wide in total. The block has three internal voids as
473 displayed in **Figure S6**. The total external volume of the acrylic body was 44.8 mL with an internal
474 operative volume of 14.4 mL. Two stainless-steel (S/S) plates (75 mm x 25 mm x 2.5 mm, RS
475 Components, UK) are secured on the front and back of the acrylic body using 10 M5 stainless-
476 steel screws (RS Component, UK). On one side (cathodic side), the stainless-steel plate was used
477 to hold in place a thin film of polytetrafluoroethylene (PTFE, Hansatech Instruments Ltd., UK)
478 and a carbon paper/Pt cathode ($\sim 2.5 \text{ cm}^2$, loading 3 mg cm^{-2} , Alfa Aesar 45372 Hydrogen
479 Electrode/Reformate, USA). On the other side (anodic side), the stainless-steel plate was used to
480 hold in place another thin film of polytetrafluoroethylene (PTFE, Hansatech Instruments Ltd., UK)
481 and provide a docking area in which to fasten the aluminium anode by using an M5 stainless-steel
482 screws and washers (RS Component, UK). The aluminium anode was made of 0.7 grams of fine-
483 grade aluminium wool (Rogue River Tools, USA). The aluminium electrodes were cleaned
484 according to the protocol described above³³. The complete compact Al-BPV system is shown in
485 **Figure S7**.

486

487 **Electrochemical characterisation of compact Al-BPV in laboratory-controlled environment**

488 The electrical output of the prototype Al-BPVs containing individual aluminium electrodes was
489 measured and recorded with a multi-channel MultiEmStat3 Potentiostat (PalmSense, United
490 Kingdom). The compact Al-BPV system constructed as described above was injected with

491 *Synechocystis* (36.5 nmol Chl) suspended in BG11 medium.
492 Linear sweep voltammetry from -1V to 0V was performed at a scan rate of 0.0001 V/s both in dark
493 and light conditions (illuminated from the side, $\sim 500 \mu\text{E m}^{-2} \text{s}^{-1}$ by a 3W LED, RS components,
494 United Kingdom) to derive the peak power and maximum current as shown in the power curves
495 (**Fig.1E**). The experimental run was conducted in a laboratory-controlled environment at $22 \pm 2 \text{ }^\circ\text{C}$
496 throughout the characterization process.

497 After the linear sweep voltammetry measurements, the compact Al-BPV was tested in
498 chronovoltammetry mode with an external load of 10 k Ω (two electrode system) for about 23 days
499 at 2 hours cycle (1 hour light / 1 hour dark), illuminated from the side $\sim 500 \mu\text{E m}^{-2} \text{s}^{-1}$ by a 3W
500 LED (RS components, UK) (**Fig.S8**).

501

502 **Testing the compact Al-BPV for powering the Arm Cortex-M0+ Processor in a domestic** 503 **environment**

504 After having characterised the compact Al-BPV system in controlled laboratory conditions, the
505 device was connected using crocodile clips to the negative and positive terminals of the test-chip
506 with the Cortex-M0+ microprocessor. The test-chip contained a LED to indicate whether sufficient
507 power was being drawn from the compact Al-BPV device to sustain the microprocessor's
508 operation. After observing that the LED was illuminated, the device was then left in the vicinity
509 of a window in a domestic environment (Cambridge, UK, **Fig.S10**). The test-chip board verifies
510 the operation of the processor and measures the potential and intensity of the electrical output of
511 the compact Al-BPV system. Data were transferred to the Internet-cloud via a Raspberry-pi/router
512 and the ThingSpeakTM platform was used to record and visualise the data (**Fig.S11**).

513

514 **CPU operation (computing mode and standby mode)**

515 The CPU was programmed to perform 45 minutes of computation work (computing Gaussian sum
516 with a frequency of 10 kHz) followed by 15 minutes in stand-by mode (no computation). The
517 experiment shown in **Figure 2** was entirely run following this alternating mode (computation /
518 standby). By contrast, the experiment shown in **Figure S12** included a first phase (week 0 to week
519 13) of continuous computation followed by a second phase (week 15 to week 20) of alternating
520 mode (computation / standby).

521

522 **Domestic environment and experimental setup where the compact Al-BPV was used to**
523 **power the CPU**

524 The compact Al-BPV was placed at the window sill in a living room of a domestic property located
525 in Cambridge (UK), latitude: 52.23 / 52°14'0"N; longitude: 0.1329 / 0°7'58"E (**Fig.S10**). The
526 compact Al-BPV was exposed to ambient lighting as recorded by a light probe mounted on the
527 test-chip (**Fig.2J-L**). To compensate for water evaporation through the teflon membranes (Callapg,
528 https://www.goodyearrubberproducts.com/2012pdfs/O_rings_Catalog/files/assets/downloads/page0009.pdf,
529 accessed on 13/12/2021), two to three mL of commercial still drinking water (Still
530 Spring Water, Harrogate, UK) was added every 7-10 days, depending on the rate of evaporation
531 due to variation in ambient temperature.

532
533 **CPU induced failure**

534 To test system failure a drop in temperature was forced by positioning an ice-pack near the
535 temperature probe mounted on the test-chip, causing a localised lowering of ambient temperature
536 below 5 °C, and automatically switching the powering of the CPU from the Al-BPV to the mains
537 electricity (USB powered), recording a voltage of >5V. To revert the powering of the CPU from
538 the mains electricity (USB powered) to the Al-BPV, the system would need to be reset manually.

539
540 **Optical microscopy investigations**

541 Optical microscopy images were taken with a RS PRO, 10 – 100X, res. 2M pixel, digital optical
542 microscope USB-interfaced (RS Component, UK).

543
544 **SEM – scanning electro microscopy investigations**

545 Scanning electron microscopy of bare Al filaments and filaments from AL-BPV was performed
546 using a Supra 55-VP SEM (Zeiss) in SE2-mode with a 2kV acceleration voltage. As only coverage
547 was to be investigated, no biological fixation step was conducted.

548
549 **CVs performed on a mix of aluminium hydroxide and extracellular matrix scraped from the**
550 **anode of a mature Al-BPV system**

551 Cyclic voltammetry measurements were carried out with a multi-channel MultiEmStat3
552 Potentiostat (PalmSense, UK). Small samples of the biofilm and extracellular matrix were scraped

553 from the colonised aluminium anode several months old and placed on the working electrode of a
554 Screen-Printed Gold Electrode C223BT (Aux.:Au; Ref.:Ag) / Ink BT. Working Electrode of 1.6
555 mm diameter (Metrohm, UK). A drop (200 μ L) of fresh BG11 was placed above the scraped
556 material on the printed electrodes. After 6 hours of resting, cyclic voltammetry measurements (21
557 scans) were carried out at 5 mV s^{-1} between -800 mV and 800 mV.

558

559 **Impedance electrochemical spectroscopy (EIS) and potentiodynamic sweep (PDS)** 560 **measurements**

561 All electrochemical measurements were performed in growth medium in a three-electrode cell.
562 The working electrode was bare Al filaments or filaments from a compact Al-BPV after ca. four
563 months of operation. The counter electrode was a platinum plate with a surface area considerably
564 larger than that of the working electrode, and the reference electrode used saturated Ag/AgCl.
565 Electrochemical impedance measurements (EIS) and potentiodynamic sweeps (PDS) were
566 performed in BG11 in a three-electrode cell. To ensure there was no biological activity the
567 filaments from the Al-BPV were immersed in absolute alcohol for 30 minutes prior to testing. EIS
568 and PDS were carried out after 60 min of open-circuit potential measurements. The EIS
569 measurements were carried out over a frequency range from 100 kHz to 10 mHz using
570 a 10 mV amplitude of sinusoidal variation around the E_{ocp} . The PDS measurements were carried
571 out from a cathodic negative potential of -0.250 V to a positive anodic potential of 1.5 V with
572 respect to initial E_{ocp} , at a scan rate of 0.168 mV/s. All measurements were recorded using
573 an Iviumstat.Xre potentiostat connected to an Ivium Boost current enhancer.

574

575 **Microbiome analysis**

576 Biological material in the supernatant fraction of samples was harvested by centrifugation (14,000
577 x g for 5 min) and the supernatant discarded. The anode matrix sample was gently inverted to
578 allow loosely associated biofilms to be dislodged from the aluminium wool anode. The suspended
579 material was transferred to a sterile centrifuge tube and large particulates settled-out for 10 min.
580 prior to removal of the overlying supernatant fraction. The supernatant cell pellets, particulates
581 and aluminium wool were individually snap-frozen in liquid nitrogen and stored at -80°C prior to
582 DNA extraction. Total DNA was extracted by pre-treating samples with lysozyme (250 μ g in 50
583 μ l of 10 mM Tris-HCl pH 8.0 and 1 mM EDTA for 30 min. at 37°C), then the DNeasy Plant Mini

584 kit (Qiagen) was used as recommended by the manufacturer.
585 Paired-end amplicon sequencing (PE250) of 16S rRNA genes was performed using the V3-V4
586 universal bacterial primers 341F (5'-CCTAYGGGRBGCASCAG -3') and 806R (5'-
587 GGACTACNNGGGTATCTAAT -3') using Illumina HiSeq platform (Novogene UK, Ltd).
588 Paired-end reads were split according to their unique barcodes and primers and barcodes truncated.
589 Subsequently, particulate and aluminium wool fastq paired-reads were concatenated to create a
590 single 'matrix' paired-read sample. DADA2³⁴ was used to quality filter, dereplicate and de-noise
591 truncated reads prior to chimera removal. Taxonomic inference of the 'liquid media' and 'matrix'
592 samples was based on the DADA2 implementation of the Naïve Bayesian classifier³⁵ trained using
593 SILVA 138 database release³⁶. Microbial community analysis of amplicon sequence variants was
594 performed using routines in *phyloseq* version 1.34.0³⁷ in R vers. 4.0.3³⁸. The data for this study
595 have been deposited in the European Nucleotide Archive (ENA) at EMBL-EBI under accession
596 number PRJEB46799
597 (<https://www.ebi.ac.uk/ena/browser/view/PRJEB46799>).

598 **Data availability**

599 The data that support the plots within this paper and other findings of this study are available at:
600 <https://doi.org/10.17863/CAM.74822>

602 **Supplementary References**

- 603
604 [1] C.C. Fu, C.H. Su, T.C. Hung, C.H. Hsieh, D. Suryani and W.T. Wu, Effects of biomass weight
605 and light intensity on the performance of photosynthetic microbial fuel cells with *Spirulina*
606 *platensis*. *Bioresource Technology*, 2009, **100**, 4183–4186.
607
608 [2] Y. Zou, J. Pisciotta, R.B. Billmyre and I.V. Baskakov, Photosynthetic microbial fuel cells With
609 positive light response, *Biotechnology and Bioengineering*, 2009, **104**, 5, 930-946.
610
611 [3] C.C. Fu, T.C. Hung, W.T. Wu, T.C. Wen and C.H. Su, Current and voltage responses in instant
612 photosynthetic microbial cells with *Spirulina platensis*. *Biochemical Engineering Journal*, 2010,
613 **52**, 175–180.
614
615 [4] J.M. Pisciotta, Y. Zou and I.V. Baskakov, Light-dependent electrogenic activity of
616 cyanobacteria, *PloS ONE*, 2010, **5**, e10821.
617

- 618 [5] Y. Zou, J. Pisciotta and I.V. Baskakov, Nanostructured polypyrrole-coated anode for sun-
619 powered microbial fuel cells. *Bioelectrochemistry*, 2010, **79**, 50–56.
620
- 621 [6] P. Bombelli, R.W. Bradley, A.M. Scott, A.J. Philips, A.J. McCormick, S.M. Cruz, A.
622 Anderson, K. Yunus, D.S. Bendall, P.J. Cameron, J.M. Davies, A.G. Smith, C.J. Howe and A.C.
623 Fisher, Quantitative analysis of the factors limiting solar power transduction by *Synechocystis* sp.
624 PCC 6803 in biological photovoltaic devices, *Energy & Environmental Science* 4, 2011, **11**, 4690-
625 4698.
626
- 627 [7] A.J. McCormick, P. Bombelli, A.M. Scott, A.J. Philips, A.G. Smith, A.C. Fisher and C.J.
628 Howe, Photosynthetic biofilms in pure culture harness solar energy in a mediatorless bio-
629 photovoltaic cell (BPV) system, *Energy & Environmental Science*, 2011, **4**, 11, 4699-4709.
630
- 631 [8] R. Thorne, H. Hu, K. Schneider, P. Bombelli, A. Fisher, L.M. Peter, A. Dent and P.J. Cameron,
632 Porous ceramic anode materials for photo-microbial fuel cells, *J. Mater. Chem.*, 2011, **21**, 18055.
633
- 634 [9] P. Bombelli, M. Zarrouati, R.J. Thorne, K. Schneider, S.J. Rowden, A. Ali, K. Yunus, P.J.
635 Cameron, A.C. Fisher, D. Ian Wilson, C.J. Howe and A.J. McCormick, Surface morphology and
636 surface energy of anode materials influence power outputs in a multi-channel mediatorless bio-
637 photovoltaic (BPV) system, *Phys. Chem. Chem. Phys.*, 2012, **14**, 12221–12229.
638
- 639 [10] K.S. Madiraju, D. Lyew, R. Kok and V. Raghavan, Carbon neutral electricity production by
640 *Synechocystis* sp. PCC6803 in a microbial fuel cell, *Bioresource Technology*, 2012, **110**, 214–
641 218.
642
- 643 [11] K. Raman and J.C.W. Lan, Performance and kinetic study of photo microbial fuel cells
644 (PMFCs) with different electrode distances, *Applied Energy*, 2012, **100**, 100–105.
645
- 646 [12] R.W. Bradley, P. Bombelli, D.J. Lea-Smith and C.J. Howe, Terminal oxidase mutants of the
647 cyanobacterium *Synechocystis* sp. PCC 6803 show increased electrogenic activity in biological
648 photo-voltaic systems, *Phys. Chem. Chem. Phys.*, 2013, **15**, 13611-13618.
649
- 650 [13] W. Chen, M. Lee, J.L. Thomas, P. Lu, M. Li and H. Lin, Microcontact Imprinting of Algae
651 on Poly(ethylene-co-vinyl alcohol) for Biofuel Cells, *ACS Appl. Mater. Interfaces*, 2013, **5**,
652 11123–11128.
653
- 654 [14] A.E. Inglesby, K. Yunus and A.C. Fisher, In situ fluorescence and electrochemical monitoring
655 of a photosynthetic microbial fuel cell. *Phys. Chem. Chem. Phys.*, 2013,**15**, 6903-691.
656
- 657 [15] J.C.W. Lan, K. Raman, C.M. Huang and C.M. Chang, The impact of monochromatic blue

658 and red LED light upon performance of photo microbial fuel cells (PMFCs) using *Chlamydomonas*
659 *reinhardtii* transformation F5 as biocatalyst. *Biochemical Engineering Journal*, 2013, **78**, 39– 43.
660

661 [16] C.C. Lin, C.H. Wei, C.I. Chen, C.J. Shieh and Y.C. Liu, Characteristics of the photosynthesis
662 microbial fuel cell with a *Spirulina platensis* biofilm. *Bioresource Technology*, 2013, **135**, 640–
663 643.

664

665 [17] V.M. Luimstra, S.J. Kennedy, J. Güttler, S.A. Wood, D.E. Williams and M.A. Packer, A cost-
666 effective microbial fuel cell to detect and select for photosynthetic electrogenic activity in algae
667 and cyanobacteria, *J. Appl. Phycol.*, 2014, **26**, 15–23.

668

669 [18] K. Schneider, R.J. Thorne and P.J. Cameron, An investigation of anode and cathode materials
670 in photomicrobial fuel cells, *Philosophical Transactions A*, 2016, **374**, 20150080.

671

672 [19] N. Samsonoff, M.D. Ooms and David Sinton, A photosynthetic-plasmonic-voltaic cell:
673 Excitation of photosynthetic bacteria and current collection through a plasmonic substrate, *Appl.*
674 *Phys. Lett.*, 2014, **104**, 043704.

675

676 [20] N. Sekar, Y. Umasankar and R.P. Ramasamy, Photocurrent generation by immobilized
677 cyanobacteria via direct electron transport in photo-bioelectrochemical cells, *Phys. Chem. Chem.*
678 *Phys.*, 2014, **16**, 7862-7871.

679

680 [21] F.L. Ng, S.M. Phang, V. Periasamy, K. Yunus, A.C. Fisher, Evaluation of algal biofilms on
681 Indium Tin Oxide (ITO) for use in biophotovoltaic platforms based on photosynthetic
682 performance, *PloS ONE*, 2014, **9**, e97643.

683

684 [22] F.L. Ng, M.M. Jaafar, S.M. Phang, Z. Chan, N.A. Salleh, S.Z. Azmi, K. Yunus, A.C. Fisher
685 and V. Periasamy, Reduced graphene oxide anodes for potential application in algae
686 biophotovoltaic platforms, *Sci. Rep.*, 2014, **4**, 7562.

687

688 [23] P. Bombelli, T. Müller, T.W. Herling, C.J. Howe and T.P.J. Knowles, A high power-density,
689 mediator-free, microfluidic biophotovoltaic device for cyanobacterial Cells, *Advanced Energy*
690 *materials*, 2015, **5**, 1401299.

691

692 [24] L.F. Huang, J.Y. Lin, K.Y. Pan, C.K. Huang and Y.K. Chu, Overexpressing ferredoxins in
693 *Chlamydomonas reinhardtii* increase starch and oil yields and enhance electric power production
694 in a photo microbial fuel cell. *Int. J. Mol. Sci.*, 2015, **16**, 19308-19325.

695

696 [25] S. Yoon, H. Lee, A. Fraiwan, C. Dai and S. Choi, A micro-sized microbial solar cell. *The 9th*
697 *IEEE International Conference on Nano/Micro Engineered and Molecular Systems (NEMS)*,

698 2014, 265-268.
699
700 [26] X. Wei, M. Mohammadifar, W. Yang and S. Choi, A Microscale Biophotovoltaic Device,
701 2016 *IEEE SENSORS*, 2016, 1-3.
702
703 [27] M. Sawa, A. Fantuzzi, P. Bombelli, C.J. Howe, K. Hellgardt and P.J. Nixon, Electricity
704 generation from digitally printed cyanobacteria, *Nature Communications*, 2017, **8**, 1, 1-10.
705
706 [28] L. Liu and S. Choi. Self-sustainable, high-power-density bio-solar cells for lab-on-a-chip
707 applications, *Lab. Chip*, 2017, **17**, 3817–3825.
708
709 [29] K.L. Saar, P. Bombelli, D.J. Lea-Smith, T. Call, E.M. Aro, T. Müller and C.J. Howe and
710 T.P.J. Knowles, Enhancing power density of biophotovoltaics by decoupling storage and power
711 delivery, *Nature Energy*, 2018, **3**, 75-81.
712
713 [30] M.J. Kim, S.J. Bai, J.R. Youn, Y.S. Song. Anomalous performance enhancement effects in
714 Ruthenium-based Dye Sensitized Solar Cells. *Journal of Power Sources*, 2019, **412**, 301-310.
715
716 [31] R. Rippka, R.Y. Stanier, J. Deruelles, M. Herdman and J.B. Waterbury, Generic
717 assignments, strain histories and properties of pure cultures of cyanobacteria. *Journal of General*
718 *Microbiology*, 1979, **111**, 1-61.
719
720 [32] D.J. Lea-Smith, N. Ross, M. Zori, D.S. Bendall, J.S. Dennis, S.A. Scott, A.G. Smith and C.J.
721 Howe, Thylakoid terminal oxidases are essential for the cyanobacterium *Synechocystis* sp.PCC
722 6803 to survive rapidly changing light intensities. *Plant. Physiol.*, 2013, **162**, 484–495.
723
724 [33] S. Kumari, S. Wenner, J.C. Walmsley, O. Lunder and K. Nisancioglu, Progress in
725 understanding initiation of intergranular corrosion on AA6005 aluminum alloy with low copper
726 content, *Journal of The Electrochemical Society*, 2019, **166**, C3114–C3123.
727
728 [34] B.J. Callahan, P.J. McMurdie, M.J. Rosen, A.W. Han, A.J.A. Johnson and S.P. Holmes,
729 DADA2: High-resolution sample inference from Illumina amplicon data, *Nat. Methods*, 2016, **13**,
730 7, 581-583.
731
732 [35] Q. Wang, G.M. Garrity, J.M. Tiedje and J.R. Cole, Naive Bayesian classifier for rapid
733 assignment of rRNA sequences into the new bacterial taxonomy, *Appl. Environ. Microbiol.*, 2007,
734 **73**, 5261-5267.
735
736 [36] P. Yilmaz, L. Wegener Parfrey, P. Yarza, J. Gerken, E. Pruesse, C. Quast, T. Schweer, J.
737 Peplies, W. Ludwig and F.O. Glöckner, The SILVA and All-species Living Tree Project (LTP)

738 taxonomic frameworks, *Nucleic Acids Res.*, 2014, **42**, D643-648.

739

740 [37] P.J. McMurdie and S. Holmes, Phyloseq: an R package for reproducible interactive analysis
741 and graphics of microbiome census data, *PLoS One*, 2013, **8**, e61217.

742

743 [38] R Core Team (2018). R: A language and environment for statistical computing. R
744 Foundation for Statistical Computing, Vienna, Austria. Available online at [https://www.R-](https://www.R-project.org/)
745 [project.org/](https://www.R-project.org/).